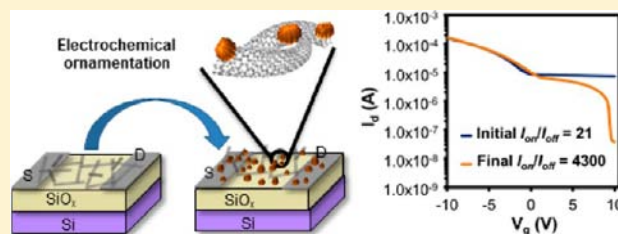


Conversion of Metallic Single-Walled Carbon Nanotube Networks to Semiconducting through Electrochemical Ornamentation

Darya Asheghali, Pornnipa Vichchulada, and Marcus D. Lay*

Department of Chemistry, University of Georgia, Athens, Georgia 30602, United States

ABSTRACT: Field-effect transistors (FETs) that incorporate single-walled carbon nanotube (SWNT) networks experience decreased on–off current ratios ($I_{\text{on}}/I_{\text{off}}$) due to the presence of metallic nanotubes. Herein, we describe a method to increase $I_{\text{on}}/I_{\text{off}}$ without the need for either specialized SWNT growth methods or post growth processing steps to remove metallic nanotubes. SWNTs that were grown using conventional arc discharge methods were deposited from aqueous suspension. Then, the SWNTs in the network were decorated with Cu_2O nanoparticles that acted as controllable valves that restricted current flow at positive gate voltages. This resulted in an unprecedented reduction in I_{off} , as the sub-10 nm sized nanoclusters acted as numerous tunable valves, providing greatly improved network sensitivity to gate voltages in the relatively small range of ± 10 V, increasing $I_{\text{on}}/I_{\text{off}}$ by up to 205-fold. Larger nanoclusters were found to increase the network conductivity but decrease $I_{\text{on}}/I_{\text{off}}$. The ability to convert metallic SWNTs to semiconducting without removing them allows for enhanced I_{on} and lower noise while still achieving greatly enhanced magnitudes of $I_{\text{on}}/I_{\text{off}}$.



INTRODUCTION

Pristine, individual single-walled carbon nanotubes (SWNTs) have excellent electrical properties that far exceed those of the semiconductors and metals currently used in microchip manufacturing. Depending on chirality and diameter, individual SWNTs may be semiconductive (s-SWNT) or metallic (m-SWNT). For s-SWNTs, the electron mobility is orders of magnitude greater than that for Si and GaAs.¹ While in m-SWNTs, the mean free path for an electron can exceed 2 μm , making them prime candidates for use as electrical interconnects. Additionally, since conduction occurs via an extended π bonding network, they are not susceptible to electromigration, which results from the movement of metal nuclei in response to momentum transfer from electrons during current flow. This is an increasingly significant failure mechanism as device structures decrease in size.² Therefore, both varieties of SWNTs have great potential in many microelectronics applications.

However, significant challenges remain for developing manufacturable electronic materials that make use of an individual SWNT as the active component, as one of the most notable characteristics of SWNTs is their polydispersity: for bulk growth processes, one-third are m-SWNTs, while the other two-thirds are s-SWNTs. Approaches to dealing with this problem include attempts at selective growth of s-SWNTs^{3–5} or post growth solution processing to remove m-SWNTs.^{6–9} However, for s-SWNTs, the band gap varies with diameter and chirality from near 0 to ~ 1.8 eV. Therefore, even after the separation of SWNTs based on their type of electrical conductivity, widely varying band gaps remain in the semiconductive portion, causing semiconductor device structures formed from individual SWNTs to be highly irreproducible.

Additionally, the current drive through an individual SWNT is limited to the nA range, while higher current drives are needed by modern electronic devices. Further, device structures based on individual SWNTs will require significant advances in the ability to control the length, orientation, and location of SWNTs during their growth or deposition.

Therefore, 2-D SWNT networks are the proximate route to their widespread use. In a 2-D array, the nanotube density and alignment largely dictate performance. Also, multiple SWNTs connected in parallel provide orders of magnitude more current than an individual SWNT. Further, unlike Si-based electronic materials, SWNT networks have great potential in transparent, lightweight, and flexible electronic materials, especially as new aqueous suspension-based deposition methods are developed for the polymer substrates used in these applications.

A drawback to the use of SWNT networks is their greatly reduced performance, relative to that observed for single-SWNT systems. This reduced performance is due to several factors that are addressed in this work: (i) Interdevice precision is low in field-effect transistors (FETs) based on SWNT networks in part because changes in the Schottky barrier height between s-SWNTs in direct contact with the metal source and drain electrodes dictate much of the response to the gate voltage (V_g),^{10–12} leaving the semiconductive channel largely unaffected. Also, the OFF-state current of SWNT network-based FETs is limited by the presence of the metallic pathways provided by m-SWNTs and small band gap s-SWNTs, since they are largely unaffected by V_g . These effects combine to increase the OFF-state source/drain leakage currents in

Received: November 30, 2012

Published: April 22, 2013

SWNT-based devices, greatly reducing their energy efficiency. (ii) Due to the inter-SWNT tunnel junctions that must be traversed in a network, their electron mobility decreases up to 3 orders of magnitude, relative to that for individual nanotubes.^{1,13} (iii) The poor attractive forces between metals and the π bonding network in nanotubes result in nonohmic contacts, increasing contact R and thereby reducing the level of ON-state current efficiency that can be achieved at a given source/drain voltage, reducing the ON-/OFF-state current ratio ($I_{\text{on}}/I_{\text{off}}$). The approach to overcoming these three challenges is described in detail below.

To address issues related to the variability in conduction for SWNTs (i), electrodeposition was used to form numerous V_g -tunable contacts composed of high work function nanoclusters along the SWNT sidewalls. This facilitated much greater coupling between the nanotube network and V_g , as occurs in conventional Si-based FETs, allowing several orders of magnitude in the reduction of I_{off} that could be achieved. This was facilitated by decorating the network with nanoclusters of the high work function species Cu_2O ($\Phi = 4.9$ eV).¹⁴ This value is slightly higher than the experimentally determined work function of 4.6–4.8 eV for SWNT films.¹⁵ High work function adsorbates withdraw electron density from s-SWNTs at the point of contact, increasing their band gap on a local level and their sensitivity to gate voltages. Cu_2O is readily formed via electrochemical methods and has been widely investigated for use in solar cells,^{16,17} sensors,^{18,19} and catalysis.^{20,21} The π network in SWNTs is strongly affected by molecular adsorbates, with a molecular electron-withdrawing species increasing the nanotube's semiconductive character by increasing its band gap on a local level.

This manuscript also presents evidence that a band gap can be opened in m-SWNTs, obviating the need to separate them from s-SWNTs before network formation. This will greatly simplify network formation and optimization. In fact, OFF-state source/drain leakage currents were greatly reduced, resulting in a 205-fold increase in $I_{\text{on}}/I_{\text{off}}$. As the effect of metallic pathways on I_{off} is reduced, networks of increased density may be deposited without sacrificing $I_{\text{on}}/I_{\text{off}}$, facilitating the advantages in reproducibility and current drive provided by greater numbers of SWNTs.²² This apparent conversion of m-SWNTs is attributed to the fact that they are not true metals, but in fact zero band gap semiconductors, or semimetals, like graphene.^{23,24} Therefore, our deposition method for metal oxide nanoclusters is an effective way to open a band gap in m-SWNTs by inserting a point where the conductivity can be controlled along an otherwise conductive nanotube (U.S. patent application).²⁵

The inter-SWNT tunnel junction (ii) is unique to network devices. At these junctions, surface-bound SWNTs have a slightly increased contact area to each other due to a slight deformation of the tubes caused by van der Waals attractions. However, since the tunneling probability for an electron decays exponentially with distance, the 3.5 Å van der Waals spacing between crossed nanotubes presents a nontrivial barrier. Additionally, Schottky barriers between m- and s-SWNTs present numerous high- R barriers in a network.^{26–28}

In this work, inter-SWNT R was reduced by depositing low defect, unbundled nanotubes in a manner that allowed control over the density and alignment of SWNTs in the network. Inter-SWNT R is greatly reduced for a network composed of individual nanotubes, compared to bundles.²⁹ Therefore, we employed a new method for producing suspensions of

unbundled high aspect ratio SWNTs and depositing them without allowing bundle formation,³⁰ while maintaining strict density control over the network during all states of its formation.^{31,32} Density control is important because as density increases, conductivity, current drive, $I_{\text{on}}/I_{\text{off}}$ and reproducibility increase. However, at very high nanotube density, the electron mobility and $I_{\text{on}}/I_{\text{off}}$ begin to decrease due to bundle formation and charge shielding.³³ Further, this deposition method allowed large number of SWNTs to be deposited either in a random orientation or with partial alignment.³⁴ The ability to increase the SWNT alignment allowed the number of inter-SWNT tunnel junctions to be reduced, maximizing the advantages in electron mobility provided by the high aspect ratio SWNTs.

Recent computational studies by Li and Marzari found that while the inter-SWNT van der Waals distance is 3.5 Å, the C-transition-metal atom distance is 2.4 Å.³⁵ This is a significant reduction in distance, considering the exponential dependence of tunneling current on the barrier distance. They also reported that the Cu–C bond was found to have a very low binding energy (0.38 eV), due to the full d-orbitals in Cu, and that transition metals with low binding energies with C had greater quantum conductance near the Fermi level between crossed s-SWNTs. Therefore, the electrodeposition of randomly distributed Cu-containing nanoparticles is expected to produce nanoparticles that fortuitously bridge inter-SWNT junctions and reduce inter-SWNT R by reducing the tunneling barrier distance between s-SWNTs and the Schottky barrier height between m-SWNTs and s-SWNTs.

Optimizing electron transfer across heterojunctions (iii) is an important consideration for incorporating any nanomaterial into conventional device structures. For SWNTs, this is complicated by difficulties with forming low-resistance metal–C bonds due to the poor “wetting” of sp^2 -hybridized C by most transition metals and Schottky barriers between s-SWNTs and metals.³⁶ This reduced attraction between metals and SWNTs leads to an increased electron tunnel barrier, increasing the R at source and drain contacts. An additional obstacle to interfacial transport is presented by the semiconductive variety of SWNTs, due to the formation of a Schottky barrier at their contacts to metal electrodes severely limiting the transistor ON-state current I_{on} .

Interfacial R was reduced as electrodeposited nanoclusters effectively nanosoldered the metal/SWNT junctions, providing an increased contact area to all SWNTs and a reduced Schottky barrier height to s-SWNTs. The reduced C-transition-metal atom distance expected for the Cu oxides allowed them to act as low resistance “shunts” that facilitated electron transfer to/from metal source and drain electrode pairs. This addresses a critical concern, as interfacial contacts often dictate the electrical properties of SWNT-based systems, rather than the enhanced properties of nanotubes.³⁷

Previous efforts to reduce the interfacial R between SWNTs and metals often involved high-temperature annealing. For example, chemical reactions between SWNTs and various metal carbides were driven at temperatures above 900 °C to form nanotube-carbides, reducing R to approximately one-fourth of its original value.³⁸ In another instance, resistive heating of a gold electrode was used to effect “local melting,” in order to embed multiwalled carbon nanotubes (MWNTs) into the electrodes.³⁹ The R was reduced by 60%, with the effect being attributed to increased interfacial contact area to the MWNT. A 5-fold increase in current was also achieved by using the

electron beam in a scanning electron microscope to solder MWNTs to Au electrodes by decomposing a gas-phase gold–C precursor.⁴⁰

A recent report by this group revealed that controlled chemical oxidation, followed by annealing at just 300 °C, could greatly improve the conductivity in SWNT networks.⁴¹ The order in which the various device structures were formed played a crucial role in the extent to which R could be reduced during postfabrication treatments. When electrical contacts were deposited on top of pre-existing networks, a moderate level of R reduction was observed. This indicates that when the metal/SWNT contacts were closed to further chemical reactions, the only reduction in R observed was that due to the enhanced inter-SWNT contacts formed during annealing. This was confirmed by Raman microscopy, which indicated a reduction in the density of sidewall defects in SWNTs and the desorption of residual dopants. However, when the network was deposited on top of prefabricated Ti electrodes, a 13-fold reduction in R and an 18-fold increase in the interdevice precision could be ascribed to the formation of “molecular anchors” at the inter-SWNT and metal/SWNT junctions. Evidently, the large contact area over which there was chemical access to the metal/SWNT interface, relative to device structures with nanotubes buried in metal electrodes, allowed for greater optimization of the interface. The chemical access provided by depositing SWNTs onto prefabricated Ti electrodes also provides a unique opportunity to use electrodeposition to increase electronic transport properties.

In order to test an electrochemical approach to device optimization, Ti electrodes were formed on a variety of silica-terminated surfaces. SWNTs do not readily adhere to native silica or Ti surfaces. However, the native oxide that formed on Ti in air resulted in a titania-terminated surface, which like silica was amenable to modification via self-assembled monolayer (SAM) formation by a silane. Therefore, all surfaces were treated with a silanization agent to form a SAM that served as an adhesion layer. Then, electrodeposition was used to form conductive shunts through the silane and the native TiO_x adlayers, bridging the electron tunneling gap between SWNTs and the conductive Ti below. To simplify the discussion of these titania surfaces, they will be referred to as Ti/TiO_x . Although Ti/TiO_x was used for these studies, this method is expected to significantly improve interfacial electron transport between SWNTs and other metals that form native oxides, like Al, Ta, Ni and various ferrous systems. Additionally, interfacial contacts to metals that do not form native oxides would also be improved via the increased contact area provided by the conductive nanoparticles that coat the SWNTs. Cu^{2+} was used for electrodeposition in these studies since its oxides form readily in an electrochemical environment and they are p-type, wide band gap semiconductors, like SWNTs. Also, the copper oxides have high work functions, which allow them to serve as electron-withdrawing dopants when in close contact with nanotubes.

The electrochemical nanosoldering method described in this manuscript is a room temperature, inexpensive, and facile route to obtaining great gains in conductance and $I_{\text{on}}/I_{\text{off}}$ since it specifically decorates the SWNTs and metal electrodes with nanoclusters of controllable size distributions. This is facilitated by control over the magnitude of the driving force for the metal deposition (via the electrochemical potential) and precise control over the average size of the nanoparticles (via the charge that is allowed to pass). Further, electrodeposition is a

nonline-of-sight deposition method that prohibits deposition on nonconductive parts of the surface, allowing preferential deposition at defect sites on individual SWNTs dispersed on insulating substrates. These abilities provide distinct advantages over physical vapor deposition methods, which indiscriminately deposit molten metal nanoparticles over the entire sample.

■ EXPERIMENTAL DETAILS

Substrate Preparation. A dual-filament thermal evaporator (Thermionics), operating under high vacuum ($P < 1 \times 10^{-6}$ Torr), was used to deposit 150 nm of Ti (99.995% pure 1/8 in. diameter pellets, Kurt J. Lesker Company) onto either glass slides or photoresist-coated, lithographically patterned Si/SiO_x wafers. Then, the substrates were cleaned with a compressed CO_2 snow-jet. The entire samples, including the Ti/TiO_x electrodes, were modified with a silane monolayer that served as an adhesion layer for the SWNTs, using a method described previously by this group.^{30,31} Briefly, samples were immersed for 45 min in a solution of 10 mM 3-(aminopropyl) triethoxysilane (3-APTES, 99%, Aldrich) in ethanol (99.5%, absolute 200 proof, ACROS). Next, the samples were cleaned in a stream of fresh ethanol and then water. In order to ensure that excess layers of the silane were removed, the surfaces were cleaned with compressed CO_2 from a snow-jet, as this has proven effective for removing excess silane, leaving only a strongly bound monolayer on the surface.⁴²

For testing the effect of nanocluster formation on SWNT network FETs, source and drain electrode pairs were formed using standard optical lithography methods. This involved UV light exposure through a patterned quartz mask to project the pattern for the electrodes onto photoresist-coated Si/SiO_x wafers. This was followed by Ti physical vapor deposition and photoresist lift-off to yield 150 nm thick source/drain electrode pairs on top of a 500 nm thick thermally grown dielectric SiO_x layer. Prior to SWNT network deposition, these samples were modified with a silane layer, as described above.

SWNT Suspension and Network Formation. Arc discharge soot (AP grade, Carbon Solutions, Inc.) was dispersed into an aqueous 1% sodium dodecyl sulfate (SDS, J.T. Baker) solution via probe ultrasonication (Fisher Model 500) at a power density of 0.4 W/mL. These conditions have been previously demonstrated to be effective at forming stable suspensions of high aspect ratio SWNTs, while minimizing sonication induced damage to the nanotube sidewalls.⁴³ Next, a low relative centrifugal force processing method was used to separate the undamaged, high aspect ratio SWNTs from amorphous C and residual catalyst contaminates.³⁰

This group has developed an SWNT network formation method that uses iterative deposition cycles to grow a network from the bottom up, while avoiding SWNT bundle formation.³⁴ To deposit reproducible densities of unbundled SWNTs bridging the electrodes, the silanized surfaces were wet with a purified SWNT suspension, then immediately dried in a unidirectional stream of N_2 , and rinsed with copious amounts of H_2O . This deposition cycle was repeated eight times for all samples to build networks that were composed of similar densities of unbundled SWNTs, as described previously.^{31,32,34} For samples designated “aligned,” one drying direction was used to deposit SWNTs, while for “crossbar” samples an equal number of orthogonal deposition steps were used. The initial R , prior to electrochemical experiments, was $\sim 1 \text{ M}\Omega$ for all samples.

Electrochemical Setup. In order to determine the effect of the area of the SWNT network relative to the contact area provided by the metal electrodes ($A_{\text{network}}/A_{\text{Ti}}$) on the electrochemical response and change in two-terminal R , samples of various dimensions were analyzed in either sealed glass beakers or homemade glass electrochemical cells, as described below. The glass cells employed a Viton gasket at the bottom that restricted the working electrode's area to a 1.0 cm diameter disk. All cells were purged with high-purity N_2 for at least 30 min prior to all experiments. Solutions were composed of 0.1 M CuSO_4 and 0.1 M H_2SO_4 (Aldrich) in ultrapure water (18.2 M Ω , Millipore). Standard three-electrode electrochemical cells, with each sample serving as the working electrode, were connected to a

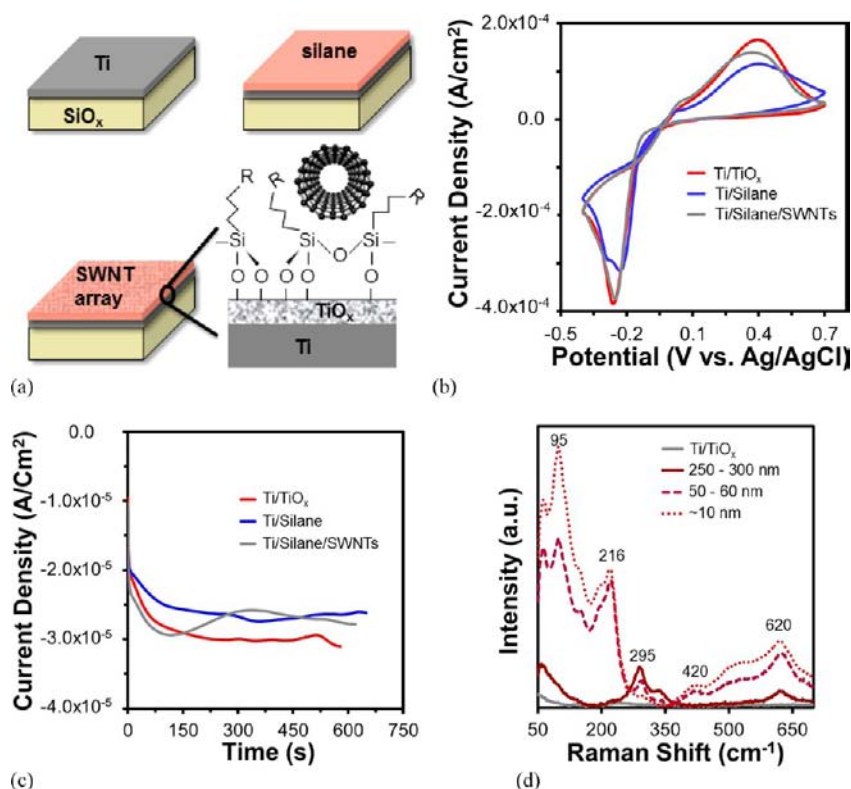


Figure 1. Electrochemical samples consisted of (a) Ti/TiO_x, TiO_x/silane, or TiO_x/silane/SWNT samples of equal surface area. (b) Representative CVs of the three surfaces showed enhanced reductive currents for the TiO_x/silane/SWNT surfaces, relative to the TiO_x/silane samples, indicating that the SWNTs facilitated the reduction of Cu. (c) The *i* vs *t* traces obtained at a constant potential of 0.10 V vs Ag/AgCl, for a total of 16.7 mC of charge, displayed a sigmoidal shape for the TiO_x/silane/SWNT samples, indicative of enhanced instantaneous and progressive nucleation processes. (d) Raman microscopy revealed that the Cu species varied with the nanoparticle size.

potentiostat (CH Instruments, 600C), with a Au wire serving as a counter electrode and a Ag/AgCl reference electrode (3 M KCl, BASi). A scan rate of 50 mV/s was used for all cyclic voltammetry (CV).

Analytical Methods. Atomic force microscopy (AFM) was performed in air using intermittent contact mode (Molecular Imaging, PicoPlus). To determine the effect of various electrodeposition conditions on the density and height of the nanoclusters, at least five areas of each sample were analyzed with AFM image analysis software (WSxM, v5.0).⁴⁴ Raman spectroscopy (Thermo Scientific, DXR SmartRaman) was performed on samples using a 532 nm laser excitation source with 5 mW intensity at the sample, 100× objective, and a charge-coupled detector. A semiconductor characterization system (Keithley, 4200SCS) and a probe station (Signatone, S-1160A) were used to ascertain the effect of nanoparticle size on two-terminal *R* and transistor performance.

RESULTS AND DISCUSSION

Electrochemistry of Cu²⁺ on Modified Ti/TiO_x Surfaces. The ~20 Å thick native oxide that spontaneously forms on fresh Ti surfaces exposed to air is largely composed of TiO₂, which is essentially an insulator since it has a band gap of 3.7 eV.⁴⁵ Crystalline forms of this passivation layer are of interest as a dielectric material in electronic device structures.⁴⁶ In these studies, thermal evaporation was used to form amorphous Ti layers with native oxides that were highly inhomogeneous, characterized by numerous grain boundaries and defects. Previously reported conductive atomic force microscopy (C-AFM) studies of polycrystalline Ti/TiO_x electrodes showed that TiO₂ layers over grain boundaries between crystals in the underlying Ti had a more than 200-fold increase in conductivity

compared to layers over crystal facets.^{47,48} They were only able to estimate the size of conductive hotspots at <50 nm, due to the resolution limits imposed by the C-AFM probe.

The electrochemical response of Ta electrodes (terminated by a 25 Å thick native oxide) was found to be defined by microscopic electrochemically active low valence oxide defects in a largely dielectric layer.⁴⁷ In the case of the Ti surfaces described herein, low valence Ti oxides (Ti₂O₃ and non-stoichiometric TiO) existed as shunts through the dielectric TiO₂ adlayer. Metallic conduction is observed for the nonstoichiometric Ti oxides which have a Ti/O ratio of 0.8–1.7.⁴⁹ The amorphous Ti/TiO_x surfaces used in these studies are expected to have numerous subnm-sized electrochemically active hotspots that represent conductive shunts to the underlying Ti. These shunts, when electrically connected to SWNTs, provide a valuable route to reducing the interfacial *R* in device structures.

The TiO₂ oxide caused the Ti/TiO_x samples to have a smaller electrochemically active surface area, as the conductive defects acted as an array of connected nanoelectrodes. This resulted in the nucleation and growth of numerous nanoparticles, rather than the formation of the conformal monolayers observed on noble metal surfaces. Ti/TiO_x surfaces were investigated at every step of the surface preparation process as follows (Figure 1a): the unmodified Ti/TiO_x surface, the silane-modified surface (TiO_x/silane), and the silane-modified surface with adsorbed SWNTs (TiO_x/silane/SWNTs).

Numerous Ti/TiO_x samples were prepared as described above and mounted in a cell that restricted the electrochemi-

cally active area to 1 cm². Freshly made samples were used for each electrochemical experiment, and AFM analysis of deposits demonstrated that the density of nucleation points was similar for all samples of Ti/TiO_x. As each CV started at the equilibrium potential, 0.35 V, and progressed at 50 mV/s in the negative (cathodic) direction, a large peak between -0.20 and -0.30 V corresponded to the reductive deposition of copper oxide nanoclusters (Figure 1b). The TiO_x/silane/SWNTs samples had increased electrochemical current for these cathodic waves, relative to the TiO_x/silane samples. Evidently, the presence of the highly conductive SWNTs provided an increased density of nucleation points, resulting in the deposition of greater densities of nanoparticles and commensurately higher current.

Each cathodic scan ended at -0.4 V, where the scan direction was reversed, and an anodic scan (toward positive potentials) began. Initially, the magnitude of reductive current remained high enough to cause each anodic curve to cross the cathodic scan at two points, near -0.16 and -0.02 V. While this behavior would be unusual for the electrodeposition of a conformal layer on a flat, noble metal surface, it is commonly observed for electrodeposition on metal oxide-terminated surfaces. Such crossover points are caused by nucleation and growth processes enhancing the electrode area, and thus the deposition current.^{50,51}

As the anodic scan continued, the large wave around 0.4 V represented the oxidation of surface-bound species to form CuO_(s) and Cu²⁺_(aq). For the Ti/TiO_x samples, the amount of charge flow was 9539 and 1300 mC in the cathodic and anodic waves, respectively. The larger magnitude of the cathodic current indicated that the complete oxidative dissolution of CuO did not occur. Potentials positive enough to facilitate complete oxidation of CuO would have further oxidized the Ti/TiO_x surface,^{50,52} increasing the thickness of its native oxide and the interfacial *R* between the SWNTs and electrode. The amount of current for the deposition of nanoparticles decreased notably for the TiO_x/silane samples, relative to the Ti/TiO_x samples. This was due in part to the silane effectively reducing the active electrode area by inhibiting access to the conductive shunts in the Ti/TiO_x surface.

After CV revealed the potentials at which nanoparticle deposition occurred, constant potential deposition (chronoamperometry) at 0.10 V vs Ag/AgCl was used to obtain information regarding the reaction rate on each surface. The amount of charge allowed to flow was limited to 16.7 mC for each surface, as this allowed the growth of nanoparticles of sufficient size to be characterized with AFM, as discussed subsequently. As 0.10 V is just negative of the equilibrium potential (0.35 V), the reaction rate was slow and the shape of the extended *i* vs *t* curves could be examined to determine the effect of each surface treatment on the transient current response observed (Figure 1c). The Ti/TiO_x samples had the highest current density, followed by the TiO_x/silane samples due to inhibition of electron transfer caused by the silane monolayer, as was the case for CVs. However, the TiO_x/silane/SWNT samples differed markedly with respect to the other samples, as the *i* vs *t* curves had a sigmoidal shape that indicated the initial nucleation process was enhanced. Then, the current reached a brief diffusion-limited regime that was followed by a broad wave of increasing current density. Additional experiments revealed that this increase in current continued indefinitely for the TiO_x/silane/SWNT samples.

Metals that are not terminated by oxide layers (i.e., Au, or Pt) typically have *i* vs *t* traces with an initial spike in current, followed by an extended region of steady-state current. This initial current spike is due to the charging of the electric double-layer and the immediate reaction of electroactive species at the electrode's surface, while in the steady-state region, deposition is limited by the rate of diffusion of the analyte to the electrode. Alternatively, unique chronoamperometric current transients are often observed during electrodeposition at heterogeneous metal oxide surfaces,⁵³ where an initial spike in current indicates instantaneous nucleation. This is followed by a broad sigmoidal feature that is typical of progressive nucleation (the density of nucleation sites increases with time), in addition to growth, resulting in continually increasing current density. This sigmoidal feature is typically observed at high driving forces (more negative potentials) for the reaction, so its observation for the TiO_x/silane/SWNT samples indicated that the SWNT enhanced the nucleation process. Then, at longer deposition times, continually increasing current is expected due to the continuously increasing electrode area.

Electrodeposited Cu microstructures are known to exist as composites of Cu, Cu₂O, and CuO, with Cu₂O being the dominate species.^{54,55} In our work, Raman microscopy indicated that the nanoparticles existed as Cu₂O, CuO, or Cu nanoparticles for small, intermediate, and large charge densities, respectively (Figure 1d). For electrodeposition on Ti/TiO_x substrates, size gradients were observed for the nanoparticles, with the size decreasing with increasing distance from the point of contact for the working electrode. This can be attributed to the electrical resistance in the Ti/TiO_x samples caused by numerous grain boundaries in these amorphous samples, and the various inclusions and defects at the surface. For the smaller nanoparticles, confocal Raman spectra had peaks expected for scattering at phonons in Cu₂O, at 95, 216, and 420 cm⁻¹.^{18,56} As the size of the nanoclusters increased, these peaks decreased in intensity, and a wave at 295 cm⁻¹, indicative of CuO,⁵⁷ increased in prominence. Cu₂O and CuO have overlapping Raman active phonons at 620 cm⁻¹. While an observable spectrum was not obtainable for the sub-10 nm clusters that were deposited in these studies, they are assumed to be largely composed of Cu₂O.

The inhomogeneous nature of the native oxide layer in these samples resulted in conductive TiO and Ti₂O₃ shunts through the nonconductive TiO₂ adlayer. TiO, in particular, exhibits metallic conduction,⁵⁸ but defects at grain boundaries in these samples also provided conductive shunts to the underlying Ti. The examination of numerous Ti/TiO_x deposits with AFM allowed visualization of the density of conductive shunts, as evidenced by the presence of nanoparticles (Figure 2). A histogram of the height information obtained in every pixel of the image, or *z*-range, revealed that the average height increased from 6.83 nm (image not shown) to 20.69 nm, with a maximum height of 115.27 nm.

For the TiO_x/silane samples, a larger density but smaller size of nanoparticles was observed under identical deposition conditions. Also, their spatial distribution decreased, with closely spaced clusters appearing throughout each AFM image (Figure 3). The average height in this representative image decreased to 13.97 nm, with a maximum of 84.51 nm. These observations can be explained by the silane monolayer acting as a defect-prone dielectric layer on the conductive shunts in the electrode, increasing the electrode/electrolyte separation by ~7 Å,⁵⁹ the monolayer thickness for 3-APTES. Due to the surface

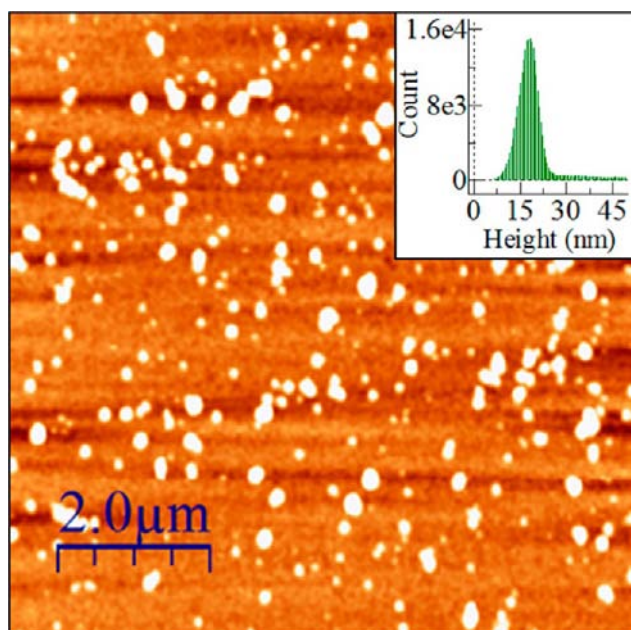


Figure 2. Representative AFM micrograph ($8 \times 8 \mu\text{m}$) showing nanoparticle growth on the Ti/TiO_x surface after deposition at 0.10 V for a charge of 16.7 mC. Each nanoparticle reveals the location of a conductive pinhole (low valence Ti oxide or conductive grain boundary) through the dielectric TiO_2 surface.

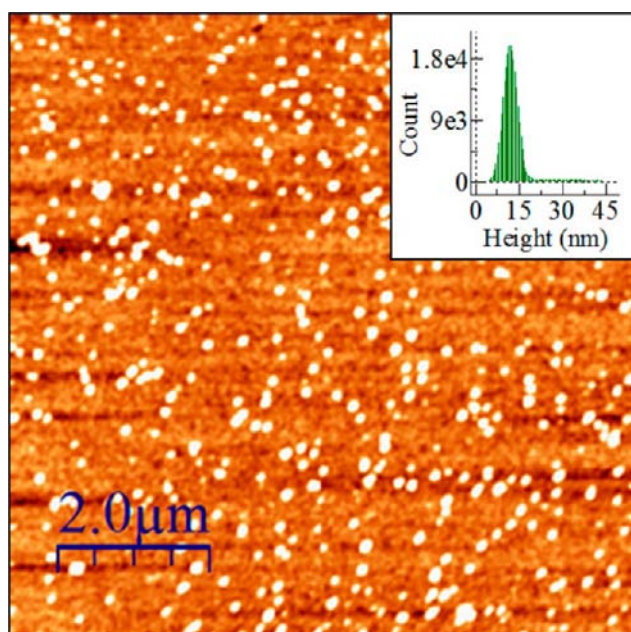


Figure 3. Representative AFM image ($8 \times 8 \mu\text{m}$) of the $\text{TiO}_x/\text{silane}$ samples showing how the addition of a silane monolayer resulted in smaller and more closely clustered nanoparticles than those observed on the Ti/TiO_x surface.

roughness of the Ti/TiO_x samples, the silane was expected to have few cross-linkages between monomers and to be characterized by a high defect density. This resulted in a larger number of smaller diameter conductive pinholes through the silane, which were revealed by the location of the nanoparticles. This resulted in closely spaced clusters of smaller Cu_2O nanoparticles, relative to those observed on the Ti/TiO_x surface.

While the presence of a silane monolayer inhibited electrodeposition on Ti/TiO_x , the $\text{TiO}_x/\text{silane}/\text{SWNT}$ samples had much larger nanoparticles, with many observed to preferentially deposit along the sidewalls of the nanotubes (Figure 4a). Nanoparticles that connect multiple SWNTs also likely provide low- R tunnel barriers that improve inter-SWNT conduction (Figure 4b). The average height observed in a representative image increased from 13.97 nm for the $\text{TiO}_x/\text{silane}$ samples to 18.85 nm, with a maximum of 111.11 nm. AFM image analysis software was used to estimate the volume occupied by the nanoclusters by summing the quotient of the x , y , and z distances measured for each point higher than 1 nm on the surface. As the same charge and electrochemical conditions were used to form these three types of deposits, they were expected to have similar amounts of material deposited, despite their clear differences in morphology. Analyzing the volume occupied by these nanoclusters provided insight into the effect of the surface properties on the charge efficiency for deposition on each surface. The volume occupied by deposits for the three surfaces were 1.3, 0.83, and $1.1 \mu\text{m}^3$, for the Ti/TiO_x , $\text{TiO}_x/\text{silane}$, and $\text{TiO}_x/\text{silane}/\text{SWNT}$ surfaces, respectively. The decreased amount of nanoclusters on the $\text{TiO}_x/\text{silane}$ samples may be attributed in part to the strong silane/ TiO_x bond disrupting the local oxidation state of the Ti/TiO_x surface, thus increasing the density of conductive shunts. Also, the silane monolayer increased the distance between the electrolyte/electrode interface. This would effectively decrease the interfacial capacitance and result in the need for greater charging current to achieve the applied electrochemical potential, decreasing the current efficiency for nanoparticle formation. This effect is expected to be lessened for the $\text{TiO}_x/\text{silane}/\text{SWNT}$ samples since the nanotubes provided a high-capacitance electrode through which more efficient electrodeposition could occur. The formation of these conductive nanoclusters presents an important opportunity to reduce the interfacial R caused by the weak attraction between sp^2 hybridized C and metal electrodes. This possibility will be explored in a subsequent section.

Electrochemistry of SWNT Networks. In order to investigate the effect of the electrodeposition of nanoparticles on the two-terminal R of networks, an SWNT network was deposited across two Ti/TiO_x electrodes that were bridged by an insulating glass substrate (Figure 5a). This configuration approximates that of the source and drain electrodes found in field-effect transistors. The devices were constructed so that two Ti/TiO_x electrodes with a combined area of 1.5 cm^2 were separated by a 1.0 cm insulating gap with an area of 2.5 cm^2 . After each sample was silanized, a network composed of similar densities of either partially aligned or crossbar oriented SWNTs was deposited. Finally, electrodeposition at 0.10 V was performed until a total charge of 16.7 mC passed (Figure 5b). The aligned network reached this charge at 2908 s, while the crossbar network required only 2026 s. Chronoamperometry curves for the two types of networks differed, with the crossbar networks having higher current densities.

At the instant a macroscopic planar electrode is polarized at a potential where an electroactive species is reduced, there is a spike in current due to the flow of an initial charging current and the commensurate reaction of the electroactive species in the immediate vicinity of the electrode. While the charging current decays exponentially with time, the diffusion-limited current from the analyte decays more slowly until a steady-state

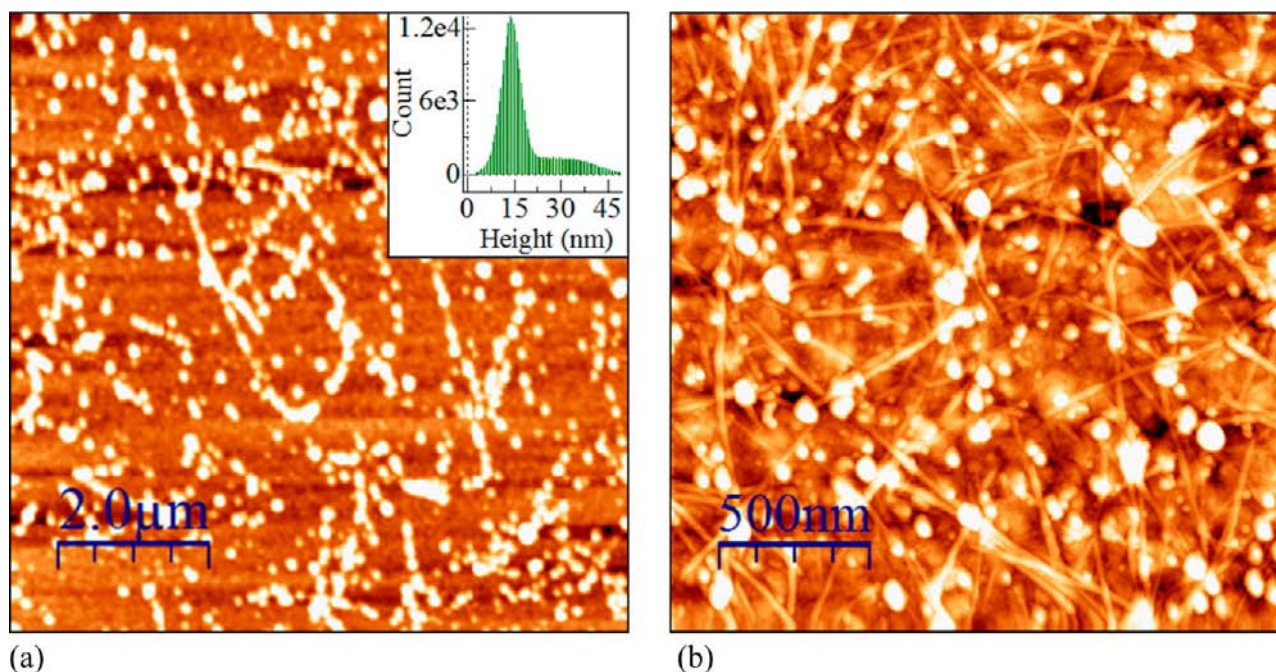


Figure 4. (a) Representative AFM image ($8 \times 8 \mu\text{m}$) of a $\text{TiO}_x/\text{silane}/\text{SWNT}$ sample showing that the deposition of a low-density network of SWNTs provided nucleation points for Cu_2O along the conductive sidewalls of the nanotubes, as observed from the greatly increased density of nanoparticles observed. (b) High-resolution AFM image showing that the Cu_2O nanoclusters also provide low- R connections between nearby SWNTs. This presents a unique opportunity to decrease the interfacial R at SWNT/metal electrode interfaces.

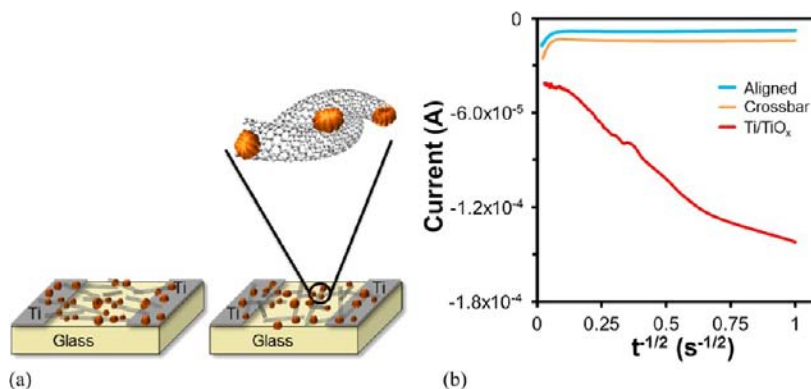


Figure 5. (a) The effect of Cu nanoparticle deposition on the two terminal R of aligned (left) and crossbar (right) networks (schematic, not drawn to scale). (b) Cottrell plots (i vs $t^{-1/2}$) of the transient current response recorded during nanoparticle growth showed that when the charge allowed to pass was limited to 16.7 mC, Ti/TiO_x samples behaved as macroscopic electrodes, while the electrochemically isolated SWNT networks behaved as an array of nanoelectrodes.

level is reached. This decay is described by the Cottrell equation:⁶⁰

$$i = \frac{nFAC\sqrt{D}}{\sqrt{\pi t}} \quad (1)$$

where i is current, n is the number of electrons transferred per electroactive ion or molecule, F is the Faraday constant, A is the area of the electrode, C is the bulk concentration of the electroactive species, D is its diffusion coefficient, and t is the time in seconds. This equation describes how the diffusion-limited current observed at a macroscopic electrode decays as a function of the inverse square root of time, as the other factors are constants. Then, a plot of i vs $t^{-1/2}$ is expected to lead to a linear regression with a current that approaches zero at very long times. The slope of this line is proportional to the square root of the diffusion coefficient for the electroactive species.

Even though the Ti/TiO_x electrodes are electrochemically active only at the conductive shunts through the TiO_2 adlayer, at long times (i.e., $t^{-1/2} < 0.6$) they behaved as planar macroscopic electrodes of an area that included the shunts, and the insulating part of the surface as the diffusion layers for each conductive shunt (each having enhanced, hemispherical diffusion) grew and overlapped to form one large zone from which the Cu^{2+} could diffuse.⁶¹ The slight nonlinearity near $t^{-1/2} = 0$ is due to convective currents. At short times, the current density was limited to the sum of the small diffusion fields that surrounded each conductive shunt, reducing the effective area of the electrode to that expected for an electrically connected array of nanoscaled electrodes separated by inert surroundings. Also, at short times, capacitive charging currents (non-Faradaic) contributed significantly to the current response, as the volume of electrolyte that contributed to

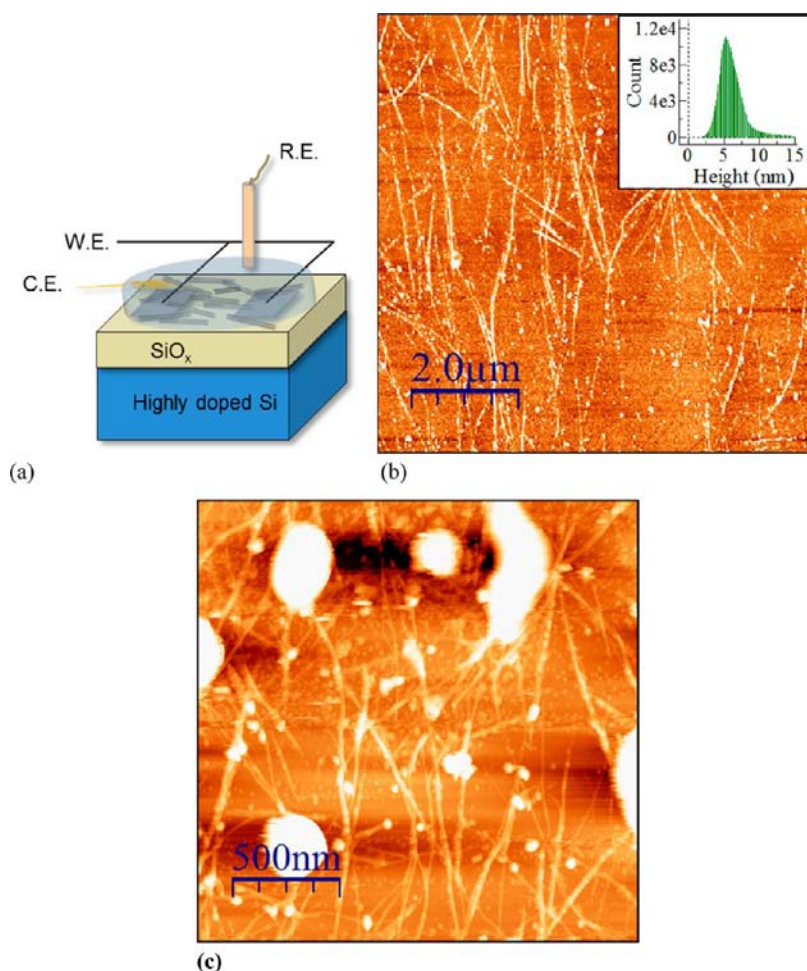


Figure 6. (a) The source/drain electrode pair, and the SWNT network between, served as the working electrode during the electrodeposition of various amounts of Cu_2O nanoparticles at 0.10 V vs Ag/AgCl. The charge was used to tune the amount of metallization that occurred. (b) Sub-10 nm sized Cu_2O nanoparticles were consistently observed on the SWNTs that bridged the source/drain channel between the Ti/TiO_x electrodes. (c) High-resolution AFM image showing that the electrodeposited nanoparticles bridge neighboring SWNTs, thus allowing reduced electrical resistance.

them was much larger than the diffusion layer. However, the capacitive current decayed exponentially with time, while the diffusion layer for each nanoelectrode slowly grew, resulting in linear diffusion. As linear diffusion began to dominate, there was an increase in the slope of the line for the Ti/TiO_x sample at $\sim t^{-1/2} = 0.6$. To put it simply, at short times the current essentially represented the combined area of the each isolated shunt and non-Faradaic processes, while at longer times, the current was more representative of the diffusion-limited reduction of Cu^{2+} at a homogeneous macroscopic planar electrode.

An examination of the linear regressions for the SWNT networks provided a clear indication of the difference in their electrochemical performance, relative to the Ti/TiO_x system. The Cottrell equation assumes that planar diffusion is the only significant contributor to mass transport. However, as these SWNT arrays were interconnected cylindrical nanoelectrodes where hemispherical diffusion of Cu^{2+} to electrochemically active defect sites dictated the current response, hemispherical diffusion dominated over the entire time scale of the experiments. This was due to the small driving forces used, relative to the equilibrium potential for the reduction of Cu^{2+} , the low defect density SWNTs providing widely spaced nucleation points, low density of SWNTs, and the limited size (sub-10 nm Cu_2O) of the nanoparticles that were grown.

Consequently, at the time scales used in these experiments, hemispherical diffusion dominated, unlike the planar diffusion observed for the Ti/TiO_x electrodes at long times. Since hemispherical diffusion is characterized by continued growth of the diffusion layer, this allowed each defect site to draw from an ever-expanding zone of the bulk solution. For growth periods much longer than those used in these studies, as the nanoparticles continue to grow, their diffusion layers would eventually overlap, and linear diffusion would then dominate. For the experiments displayed in Figure 5b, before diffusion layer overlap occurred, convective currents in the solutions led to increased current for $0 < t^{-1/2} < 0.1 \text{ s}^{-1/2}$. While the Ti/TiO_x samples were similarly affected by convective currents, the effect was more pronounced for the SWNT network electrodes because of their ever-expanding diffusion zones. The current response of a cylindrical nanoelectrode can be described by the equation

$$i = \frac{nFAC\sqrt{D}}{\sqrt{\pi t}} + \frac{2nFACD}{r \ln(4Dt/r^2)} \quad (2)$$

where r is the radius of the electrode. The first term was important at very short times, when planar diffusion dominated. While the second term describes the steady-state current observed at long times when hemispherical diffusion domi-

nated. When r is in the nm regime, the time it takes for the second term to dominate, and thus the time to reach a steady-state current, is very short. Additionally, as the magnitude of capacitive currents scales with electrode area, the charging current is very small for this system.

Electrochemical Growth of Nanoclusters on SWNT Networks. The reduction of defect density in suspension processed SWNTs is an important consideration for their ultimate use in electronic and structural materials. Recently, Fan and co-workers found that 3.5 M HCl treatments increased the sidewall defect density at a rate of $\sim 1/\mu\text{m}/\text{h}$ for chemical vapor deposition-grown nanotubes and that suspension processed arc discharge SWNTs had a defect density exceeding 1 per 100 nm, due to the harsh ultrasonication and acid treatments used to suspend and purify the nanotubes.⁶² In order to minimize defect density, the arc discharge soot used in these studies was processed using low power ultrasonic agitation for dispersion, followed by iterative centrifugation at low G to separate high aspect ratio SWNTs.³⁰ This resulted in stable suspensions of high aspect ratio SWNTs having low defect densities, while acid purification methods would have imparted defects that would increase electron scattering along the length of each SWNT, thus increasing R . Additionally, because defect sites are the preferred locations for nanoparticle nucleation on SWNTs, reducing the sidewall defect density increased the spacing between Cu_2O nanoparticles to a level that allowed each to act as a discrete, tunable valve. Therefore, control over the density of SWNTs in the network and their defect density obviates the need to control the location of defect sites, since varying the ultrasonication or chemical conditions used during suspension formation presents a powerful opportunity to control the overall density of nanoparticles for other electronic applications.

In order to investigate the effect of electrodeposited metal oxide nanoclusters on the $I_{\text{on}}/I_{\text{off}}$ of SWNT network-based FETs, standard lithographic methods were used to form Ti/ TiO_x electrodes on Si/ SiO_x wafer fragments so that the conductive underlying Si could be used as a gate electrode during device testing. Then, Ti/ TiO_x electrodes served as source and drain electrodes that were bridged by SWNT networks. These FETs had a channel length and width of 300 and 100 μm , respectively. While methods for aligning and coating SWNTs with metals have microelectronic and sensing applications, the focus of these investigations was the effect of Cu_2O nanoparticles on the semiconductive character of a network composed of a mixture of s - and m -SWNTs. Therefore, a deposition voltage of 0.10 V vs Ag/AgCl and charge flow limits were used to limit the size of the nanoparticles to <15 nm. The use of potentials increasingly negative of the equilibrium potential was found to increase the size of the nanoparticles until they coalesced and completely coated the individual SWNTs comprising the network.

The electrode area was confined to a 1.0 cm diameter disc that encompassed the Ti/ TiO_x electrodes. This was accomplished by mounting each sample in a homemade glass cell that housed the reference and counter electrodes. Then, the electrochemically active area was defined by the TiO_x /silane electrodes and the SWNTs in the macroscopic network that bridged the electrodes (Figure 6). A deposition charge of 16.7 mC resulted in the growth of nanoparticles on the SWNTs within the network that bridged the source/drain channel. Although they are highly conductive like metals, the sidewalls of SWNTs are inert toward electrochemical deposition of

adsorbates. Therefore, deposits generally form via the nucleation and growth of nanoclusters on defects at the ends and sidewalls of the nanotubes. On graphite, this type of preferential nucleation at defects has been attributed to the higher coordination provided by oxygen-containing defects.⁶³ For SWNTs, the nanoclusters nucleated at defects and then grew into nm-sized clusters having their size predetermined by the amount of electrochemical charge allowed to pass. Therefore, van der Waals attractions existed between the nanoclusters and sidewalls, while a stronger coordination bond, possibly containing a significant degree of covalent character, existed between the defect and the nanoclusters.

The average height observed for AFM images of unbundled arc discharge SWNTs is 1.4 nm.³⁰ The average height observed 200 μm from the TiO_x /SWNT network interface to 8.5 ± 0.3 nm. The average size of the nanoparticles decreased to 7.3 ± 0.2 nm at 2000 μm from the TiO_x /SWNT network interface. Such a gradient in nanoparticle size is typically observed in SWNT networks,^{64,65} as the SWNTs acts as a collection of low- R wires, with high R at each inter-SWNT junction causing a drop in the electrochemical potential with distance. Nanoparticle growth was not observed on isolated SWNTs or the silica substrate, indicating that electrodeposition is an effective manner to preferentially modify the SWNTs in a conductive network.

Effect of Cu_2O Nanoparticles on Electrical Resistance.

To determine the effect of Cu_2O nanoparticles on R for low-density networks of unbundled SWNTs, a semiconductor characterization unit was used to measure the two-terminal resistance by obtaining i/V curves in air for the range ± 0.1 V. For all electrochemical experiments involving FETs, the amount of Cu_2O deposited was limited by controlling the total charge allowed to flow before the cell was returned to the equilibrium potential, and the sample was removed from the cell. Control experiments, where R was measured before and after samples were immersed in the electrochemical cell and held at potentials near or slightly positive of the equilibrium potential, resulted in no appreciable changes in two-terminal R or FET response. However, the magnitude of R was observed to decrease with decreasing deposition potential. Two-point probe R measurements were used, as this configuration closely resembles that of the measurements for the FETs described below.

The change in R was strongly affected by the alignment of the SWNTs in the network. For a deposition potential of 0.1 V vs Ag/AgCl, the average R decreased from 1.420 ± 0.005 to 0.84 ± 0.02 $\text{M}\Omega$ for the "aligned" samples, representing a 41% decrease in R . The average R decreased from 1.19 ± 0.06 to 0.132 ± 0.006 $\text{M}\Omega$ for the "crossbar" samples, corresponding to a 89% reduction in R . Part of the reduction in R for both levels of alignment is attributed to the formation of ohmic contacts between s - and m -SWNTs in the network when nanoparticles bridged those junctions, reducing the Schottky barrier between the two types of conductors. The increased response of the crossbar samples can be attributed to the greater number of inter-SWNT junctions. When high aspect ratio SWNTs were oriented orthogonally, the number of junctions increased significantly. This allowed greater gains in conductivity. The effect of the density of the nanoclusters on the two-terminal R and FET performance of both types of networks is currently under investigation, but it is expected that performance gains will decrease as the density of defects on the SWNTs increases, since sidewall defects impede intra-SWNT current flow.

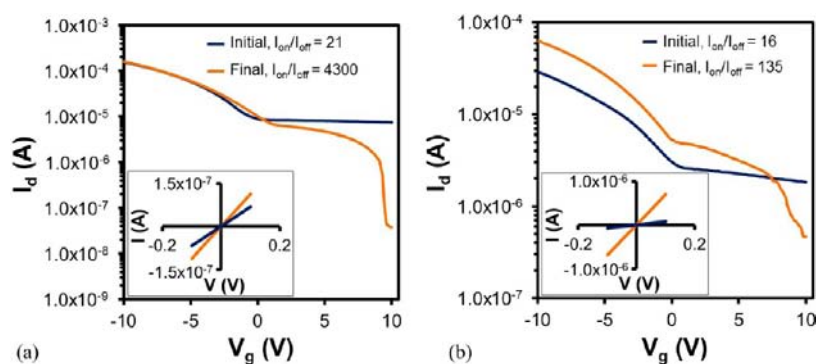


Figure 7. Representative log plots showing the dependence of the change in I_{on}/I_{off} on the alignment of SWNTs comprising the network revealed that (a) partially aligned SWNTs allowed for reduced R and greater improvements in I_{on}/I_{off} than (b) orthogonally oriented SWNTs, as the increase in I_{on}/I_{off} was 205- and 8-fold, respectively. Insets: two-terminal i/V curves obtained at $V_g = 0$ V showed that a greater reduction in R was achieved for “crossbar” networks.

Effect of Cu_2O Nanoparticles on SWNT Network Field-Effect Transistor Performance.

When the performance of “aligned” and “crossbar” samples were examined in FETs, the “aligned” samples had increased performance gains with respect to I_{on}/I_{off} . The magnitude of I_{on} and I_{off} was determined at -10 and $+10$ V, respectively. After a deposition charge of 2 mC was used to form the nanoclusters, a slight increase in I_{on} and a dramatic decrease in I_{off} were observed. The “aligned” networks consistently had the greatest increase in I_{on}/I_{off} . For the representative sample in Figure 7a, the I_{on}/I_{off} increased from 21 to 4300, representing a 205-fold increase in I_{on}/I_{off} . The “crossbar” networks had a significantly greater initial R , and I_{on}/I_{off} changed from 16 to 135, representing a 8-fold increase. At higher electrochemical charge densities, both the two-terminal R and I_{on}/I_{off} decreased, as the transistor response exhibited increasing metallic behavior for both types of networks. It was also notable that the initial R was higher for “crossbar” networks, although the density of nanotubes for the two networks was similar. This can be attributed to the fewer number of junctions that had to be traversed during electron transport when the SWNTs were partially aligned. This facilitated greater gains in two-terminal R for “crossbar” networks after nanoparticle deposition (Figure 7a,b, insets). On the other hand, the networks composed of partially aligned SWNTs provided fewer electrical pathways between the source and the drain electrodes, increasing the efficiency with which the nanoparticle valves could turn off current flow.

As unseparated SWNTs have a distribution of one-third metallic and two-third semiconductive, low-density networks of unbundled nanotubes behave as semiconductors due to the lack of metallic pathways in the network. However, at the higher densities used in these studies, the m-SWNTs formed short circuit pathways that greatly reduced the initial I_{on}/I_{off} of SWNT network FETs. Then, the OFF-state current was indicative of the number of metallic pathways through the film. Therefore, starting with FETs that exhibited a low initial I_{on}/I_{off} allowed confirmation of the fact that Cu_2O nanoparticle deposition increased the V_g sensitivity of the m-SWNTs in the conductive pathways. Park et al. have used scanned gate microscopy studies to demonstrate that point defects along m-SWNTs caused resonant electron scattering that resulted in slight sensitivity of the conductance to changes in V_g .⁶⁶

Sensitivity to V_g in m-SWNTs is possible because they are not true metals but in fact semimetals or zero band gap semiconductors, like graphene. Since graphene is a 2-D

material, efforts to open a band gap in it have centered on reducing one of its lateral dimensions and/or functionalizing its edges.^{67–69} However, the 1-D nature of SWNTs simplifies the process of band gap tuning. The electrodeposition of Cu_2O nanoparticles that increased the local sensitivity of a m-SWNT to V_g essentially inserted a controllable valve along a conducting wire. Therefore, while much of the SWNT continued to exhibit high conductivity in the presence of positive values of V_g , electrical transport was halted at each nanoparticle. The mechanism of this likely involved each high work function nanocluster depleting the electron density within a few nm of its location on the m-SWNT, essentially inducing local p-type character in an otherwise metallic or small band gap SWNT. Whenever junctions are formed between two materials with differing Fermi levels, band bending occurs in the valence and conduction bands. Then, the large electric field provided by V_g allows manipulation of this band bending and the depletion region near the junction, in order to tune the resistance of electron flow throughout the film. A discontinuity in each FET response curve marked the transition between two regions of high slope after the deposition of nanoclusters. It is likely that V_g modulated the carrier charge density in the s-SWNTs at gate voltages that were negative of the discontinuity, while more positive gate voltages turned off conductivity through the nanocluster-modified defect sites in the m-SWNTs. There are ongoing studies in this group of the mechanism behind this behavior in order to yield greater insight into this phenomenon.

CONCLUSIONS

Forming SWNT networks on prefabricated metal electrodes using liquid deposition methods provides a facile route to device assembly. This device geometry also facilitated the use of electrochemical methods to enhance the interfacial electron transport by the formation of chemisorbed Cu_2O shunts through a silane monolayer to the conductive underlying Ti. This provides greatly improved connections, compared to the weak van der Waals contacts that exist at unmodified metal/SWNT interfaces. As SAMs composed of silane were used as adhesion layers on SiO_x surfaces, the use of metal electrodes that were terminated with a thin oxide layer allowed the formation of a single silane monolayer that coated the entire surface. Then, after network formation, electrochemical methods were used to optimize the electrical properties of the thin films.

Local gating at Cu₂O modified defects on m-SWNTs was obtained, allowing greatly reduced OFF-state currents to be achieved. The great increase in $I_{\text{on}}/I_{\text{off}}$ for both types of networks indicated that metallic short circuit pathways in the networks were converted to semiconductive, as much of the increase in $I_{\text{on}}/I_{\text{off}}$ occurred via a greatly reduced I_{off} for FETs that initially showed little response to V_g . This indicated that at positive values of V_g , the Cu₂O adsorbates opened a band gap in m-SWNTs and small band gap s-SWNTs, by locally withdrawing electron density. This would effectively allow each nanoparticle/SWNT contact to act as a nanoscale valve that could be closed at positive values of V_g , allowing much lower magnitudes of $I_{\text{on}}/I_{\text{off}}$ to be achieved.

Unlike 2-D sheets of graphene, the 1-D nature of m-SWNTs provided a unique opportunity to control their electrical properties by simply attaining the capability to tune their conductivity at any one point along the tube axis. Electro-deposited metal oxide nanoclusters functioned as the formation of numerous valves needed to allow a much-enhanced response of the network to V_g . This has great potential to increase the operating efficiency of SWNT network-based electronic device structures, overall device performance is greatly improved, and less expensive gate dielectrics can be used when the sensitivity to V_g is increased. This approach also reduces the effect of metallic SWNTs in networks without the need for expensive processing steps to separate nanotubes based on their type of conductivity.

AUTHOR INFORMATION

Corresponding Author

mlyay@uga.edu

Notes

The authors declare no competing financial interest.

ACKNOWLEDGMENTS

The authors gratefully acknowledge financial support from the National Science Foundation through the Center for Nano-structured Electronic Materials, a Phase I Center for Chemical Innovation (NSF grant CHE-1038015), and NSF grant no. DMR-0906564.

REFERENCES

- (1) Zhou, X. J.; Park, J. Y.; Huang, S. M.; Liu, J.; McEuen, P. L. *Phys. Rev. Lett.* **2005**, *95*.
- (2) Taychatanapat, T.; Bolotin, K. I.; Kuemmeth, F.; Ralph, D. C. *Nano Lett.* **2007**, *7*, 652.
- (3) Zhou, W.; Zhan, S.; Ding, L.; Liu, J. *J. Am. Chem. Soc.* **2012**, *134*, 14019.
- (4) Yang, X.; Liu, L.; Wu, M.; Wang, W.; Bai, X.; Wang, E. *J. Am. Chem. Soc.* **2011**, *133*, 13216.
- (5) Hong, G.; Zhang, B.; Peng, B.; Zhang, J.; Choi, W. M.; Choi, J.-Y.; Kim, J. M.; Liu, Z. *J. Am. Chem. Soc.* **2009**, *131*, 14642.
- (6) Zhang, L.; Tu, X.; Welscher, K.; Wang, X.; Zheng, M.; Dai, H. *J. Am. Chem. Soc.* **2009**, *131*, 2454.
- (7) Palacin, T.; Le Khanh, H.; Joussetme, B.; Jegou, P.; Filoramo, A.; Ehli, C.; Guldi, D. M.; Campidelli, S. *J. Am. Chem. Soc.* **2009**, *131*, 15394.
- (8) Zhang, L.; Zanic, S.; Tu, X.; Wang, X.; Zhao, W.; Dai, H. *J. Am. Chem. Soc.* **2008**, *130*, 2686.
- (9) So, H. M.; Kim, B.-K.; Park, D.-W.; Kim, B. S.; Kim, J.-J.; Kong, K.-J.; Chang, H.; Lee, J.-O. *J. Am. Chem. Soc.* **2007**, *129*, 4866.
- (10) Byon, H. R.; Choi, H. C. *J. Am. Chem. Soc.* **2006**, *128*, 2188.
- (11) Chen, Z. H.; Appenzeller, J.; Knoch, J.; Lin, Y. M.; Avouris, P. *Nano Lett.* **2005**, *5*, 1497.

- (12) Freitag, M.; Tsang, J. C.; Bol, A.; Yuan, D.; Liu, J.; Avouris, P. *Nano Lett.* **2007**, *7*, 2037.
- (13) Rouhi, N.; Jain, D.; Burke, P. J. *ACS Nano* **2011**, *5*, 8471.
- (14) Caballero-Briones, F.; Artes, J. M.; Diez-Perez, I.; Gorostiza, P.; Sanz, F. *J. Phys. Chem. C* **2009**, *113*, 1028.
- (15) Hu, L.; Hecht, D. S.; Grüner, G. *Chem. Rev.* **2010**, *110*, 5790.
- (16) Yuhas, B. D.; Yang, P. *J. Am. Chem. Soc.* **2009**, *131*, 3756.
- (17) McShane, C. M.; Choi, K.-S. *J. Am. Chem. Soc.* **2009**, *131*, 2561.
- (18) Deng, S.; Tjoa, V.; Fan, H. M.; Tan, H. R.; Sayle, D. C.; Olivo, M.; Mhaisalkar, S.; Wei, J.; Sow, C. H. *J. Am. Chem. Soc.* **2012**, *134*, 4905.
- (19) Yang, F.; Choi, Y.; Liu, P.; Stacchiola, D.; Hrbek, J.; Rodriguez, J. A. *J. Am. Chem. Soc.* **2011**, *133*, 11474.
- (20) Li, C. W.; Kanan, M. W. *J. Am. Chem. Soc.* **2012**, *134*, 7231.
- (21) Huang, W.-C.; Lyu, L.-M.; Yang, Y.-C.; Huang, M. H. *J. Am. Chem. Soc.* **2012**, *134*, 1261.
- (22) Kocabas, C.; Pimparkar, N.; Yesilyurt, O.; Kang, S. J.; Alam, M. A.; Rogers, J. A. *Nano Lett.* **2007**, *7*, 1195.
- (23) Yan, X.; Cui, X.; Li, L.-s. *J. Am. Chem. Soc.* **2010**, *132*, 5944.
- (24) Heller, I.; Chatoor, S.; Männik, J.; Zevenbergen, M. A. G.; Dekker, C.; Lemay, S. G. *J. Am. Chem. Soc.* **2010**, *132*, 17149.
- (25) Lay, M. D.; Vichchulada, P.; Asheghali, D. U.S. Patent Application 61/733,473, 2012.
- (26) Yang, M. H.; Teo, K. B. K.; Milne, W. I.; Hasko, D. G. *Appl. Phys. Lett.* **2005**, *87*, 3.
- (27) Lu, C. G.; An, L.; Fu, Q. A.; Liu, J.; Zhang, H.; Murduck, J. *Appl. Phys. Lett.* **2006**, *88*, 3.
- (28) Fuhrer, M. S.; Nygard, J.; Shih, L.; Forero, M.; Yoon, Y. G.; Mazzone, M. S. C.; Choi, H. J.; Ihm, J.; Louie, S. G.; Zettl, A.; McEuen, P. L. *Science* **2000**, *288*, 494.
- (29) Nirmalraj, P. N.; Lyons, P. E.; De, S.; Coleman, J. N.; Boland, J. *J. Nano Lett.* **2009**, *9*, 3890.
- (30) Bhatt, N. P.; Vichchulada, P.; Lay, M. D. *J. Am. Chem. Soc.* **2012**, *134*, 9352.
- (31) Zhang, Q.; Vichchulada, P.; Lay, M. D. *J. Phys. Chem. C* **2010**, *114*, 16292.
- (32) Vichchulada, P.; Zhang, Q.; Duncan, A.; Lay, M. D. *ACS Appl. Mater. Interfaces* **2010**, *2*, 467.
- (33) Sangwan, V. K.; Ortiz, R. P.; Alaboson, J. M. P.; Emery, J. D.; Bedzyk, M. J.; Lauhon, L. J.; Marks, T. J.; Hersam, M. C. *ACS Nano* **2012**, *6*, 7480.
- (34) Zhang, Q.; Vichchulada, P.; Cauble, M. A.; Lay, M. D. *J. Mater. Sci.* **2009**, *44*, 1206.
- (35) Li, E. Y.; Marzari, N. *ACS Nano* **2011**, *5*, 9726.
- (36) Zhang, Y.; Franklin, N. W.; Chen, R. J.; Dai, H. *J. Chem. Phys. Lett.* **2000**, *331*, 35.
- (37) Rodriguez-Manzo, J. A.; Banhart, F.; Terrones, M.; Terrones, H.; Grobert, N.; Ajayan, P. M.; Sumpter, B. G.; Meunier, V.; Wang, M.; Bando, Y.; Golberg, D. *Proc. Natl. Acad. Sci. U.S.A.* **2009**, *106*, 4591.
- (38) Zhang, Y.; Ichihashi, T.; Landree, E.; Nihey, F.; Iijima, S. *Science* **1999**, *285*, 1719.
- (39) Asaka, K.; Karita, M.; Saito, Y. *Appl. Surf. Sci.* **2011**, *257*, 2850.
- (40) Madsen, D. N.; Mølhav, K.; Mateiu, R.; Rasmussen, A. M.; Brorson, M.; Jacobsen, C. J. H.; Bøggild, P. *Nano Lett.* **2002**, *3*, 47.
- (41) Zhang, Q.; Vichchulada, P.; Shivareddy, S. B.; Lay, M. D. *J. Mater. Sci.* **2012**, *47*, 6812.
- (42) Chow, B. Y.; Mosley, D. W.; Jacobson, J. M. *Langmuir* **2005**, *21*, 4782.
- (43) Vichchulada, P.; Cauble, M. A.; Abdi, E. A.; Obi, E. I.; Zhang, Q.; Lay, M. D. *J. Phys. Chem. C* **2010**, *114*, 12490.
- (44) Horcas, I.; Fernandez, R.; Gomez-Rodriguez, J. M.; Colchero, J.; Gomez-Herrero, J.; Baro, A. M. *Rev. Sci. Instrum.* **2007**, *78*.
- (45) Savio, A. K. P. D.; Starikov, D.; Bensaoula, A.; Pillai, R.; de la Torre García, L. L.; Robles Hernández, F. C. *Ceram. Int.* **2012**, *38*, 3529.
- (46) Lee, M.-K.; Yen, C.-F. *Electrochem. Solid State* **2010**, *13*, G87.
- (47) Basame, S. B.; White, H. S. *Anal. Chem.* **1999**, *71*, 3166.

- (48) Boxley, C. J.; White, H. S.; Gardner, C. E.; Macpherson, J. V. *J. Phys. Chem. B* **2003**, *107*, 9677.
- (49) Rao, C. N. R.; Subba Rao, G. V. *Phys. Status Solidi* **1970**, *1*, 597.
- (50) Emery, S. B.; Hubble, J. L.; Roy, D. J. *Electroanal. Chem.* **2004**, *568*, 121.
- (51) Oskam, G.; Searson, P. C. *Surf. Sci.* **2000**, *446*, 103.
- (52) Casillas, N.; Charlebois, S.; Smyrl, W. H.; White, H. S. *J. Electrochem. Soc.* **1994**, *141*, 636.
- (53) Scharifker, B.; Hills, G. *Electrochim. Acta* **1983**, *28*, 879.
- (54) Liu, R.; Oba, F.; Bohannon, E. W.; Ernst, F.; Switzer, J. A. *Chem. Mater.* **2003**, *15*, 4882.
- (55) Zhao, L.; Dong, W.; Zheng, F.; Fang, L.; Shen, M. *Electrochim. Acta* **2012**, *80*, 354.
- (56) Wu, S.; Yin, Z.; He, Q.; Lu, G.; Zhou, X.; Zhang, H. *J. Mater. Chem.* **2011**, *21*, 3467.
- (57) Basu, M.; Sinha, A. K.; Pradhan, M.; Sarkar, S.; Negishi, Y.; Pal, T. *J. Phys. Chem. C* **2011**, *115*, 20953.
- (58) Banus, M. D.; Reed, T. B.; Strauss, A. J. *Phys. Rev. B* **1972**, *5*, 2775.
- (59) Vandenberg, E. T.; Bertilsson, L.; Liedberg, B.; Uvdal, K.; Erlandsson, R.; Elwing, H.; Lundstrom, I. *J. Colloid Interface Sci.* **1991**, *147*, 103.
- (60) Laitinen, H. A.; Kolthoff, I. M. *J. Am. Chem. Soc.* **1939**, *61*, 3344.
- (61) Bard, A. J.; Faulkner, L. R. *Electrochemical Methods, Fundamentals and Applications*, 2nd ed.; John Wiley & Sons: New York, 2001.
- (62) Fan, Y. W.; Goldsmith, B. R.; Collins, P. G. *Nat. Mater.* **2005**, *4*, 906.
- (63) Walter, E. C.; Murray, B. J.; Favier, F.; Kaltenpoth, G.; Grunze, M.; Penner, R. M. *J. Phys. Chem. B* **2002**, *106*, 11407.
- (64) Dudin, P. V.; Snowden, M. E.; Macpherson, J. V.; Unwin, P. R. *ACS Nano* **2011**, *5*, 10017.
- (65) Day, T. M.; Wilson, N. R.; Macpherson, J. V. *J. Am. Chem. Soc.* **2004**, *126*, 16724.
- (66) Bockrath, M.; Liang, W. J.; Bozovic, D.; Hafner, J. H.; Lieber, C. M.; Tinkham, M.; Park, H. K. *Science* **2001**, *291*, 283.
- (67) Yang, Z.; Sun, Y.; Alemany, L. B.; Narayanan, T. N.; Billups, W. *E. J. Am. Chem. Soc.* **2012**, *134*, 18689.
- (68) Schwab, M. G.; Narita, A.; Hernandez, Y.; Balandina, T.; Mali, K. S.; De Feyter, S.; Feng, X.; Muellen, K. *J. Am. Chem. Soc.* **2012**, *134*, 18169.
- (69) Balog, R.; Jorgensen, B.; Wells, J.; Laegsgaard, E.; Hofmann, P.; Besenbacher, F.; Hornekaer, L. *J. Am. Chem. Soc.* **2009**, *131*, 8744.